

Express Optical Analysis of Epitaxial Graphene on SiC: Impact of Morphology on Quantum Transport

Tom Yager,[†] Arseniy Lartsev,[†] Sumedh Mahashabde,[†] Sophie Charpentier,[†] Dejan Davidovikj,[†] Andrey Danilov,[†] Rositza Yakimova,[‡] Vishal Panchal,^{§,||} Olga Kazakova,[§] Alexander Tzalenchuk,^{§,||} Samuel Lara-Avila,^{*,†} and Sergey Kubatkin[†]

[†]Department of Microtechnology and Nanoscience, Chalmers University of Technology, Göteborg, S-41296, Sweden

[‡]Department of Physics, Chemistry and Biology (IFM), Linköping University, Linköping, S-581 83, Sweden

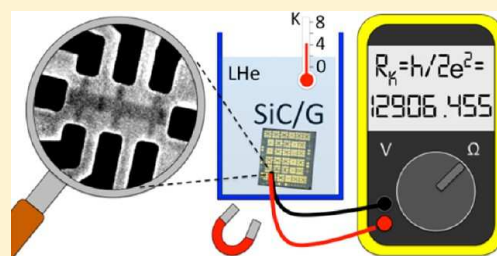
[§]National Physical Laboratory, Teddington, TW11 0LW, United Kingdom

^{||}Department of Physics, Royal Holloway, University of London, Egham, TW20 0EX, United Kingdom

Supporting Information

ABSTRACT: We show that inspection with an optical microscope allows surprisingly simple and accurate identification of single and multilayer graphene domains in epitaxial graphene on silicon carbide (SiC/G) and is informative about nanoscopic details of the SiC topography, making it ideal for rapid and noninvasive quality control of as-grown SiC/G. As an illustration of the power of the method, we apply it to demonstrate the correlations between graphene morphology and its electronic properties by quantum magneto-transport.

KEYWORDS: Epitaxial graphene, optical microscopy, electron transport, graphene characterization, graphene morphology, graphene topography



Rapid proliferation of graphene to many hundreds of research groups across the world owed in equal proportion to a simple fabrication technique by exfoliation and to its surprisingly straightforward observation by optical microscopy (OM).^{1–3} To detect atomically thin flakes, they are placed onto smooth silicon wafers coated with a dielectric of a carefully chosen thickness and illuminated with light of a matching wavelength. Interference of reflected light from the dielectric layer/Si interface (dielectric layer = SiO₂, Si₃N₄, Al₂O₃, etc.) enhances the contrast provided by graphene allowing one to distinguish even individual monolayers.^{4,5} Being intrinsically noninvasive, OM preserves the electronic integrity of graphene, which is crucial for subsequent device fabrication in both fundamental and applied studies. In seminal experiments, following the identification of graphene flakes by optical microscope, low-temperature magneto-transport revealed the quasi-relativistic nature of carriers in graphene.^{2,3} Graphene produced by other methods, such as chemical vapor deposition (CVD), that can be transferred onto a suitable substrate can be examined in a similar fashion. For this type of large-area graphene, OM serves as a quality control in terms of, for example, the domain size or the number of layers.^{6,7}

Annealing of silicon carbide (SiC) at high temperature is a reliable technique to produce monolayer graphene (SiC/G), with several proof-of-concept electronic devices already demonstrated on this material including transistors,^{8–10} sensors,^{11–14} and a quantum resistance standard.^{15,16} Research and technology of SiC/G would benefit from simple and fast

methods for graphene quality control. As there is no interference layer between graphene and SiC, the visibility of monolayer graphene was theoretically anticipated to be very weak.¹⁷ Despite the possibility to observe graphene on transparent substrates using an optical microscope in transmission or reflection mode,¹⁸ for SiC/G this type of imaging has only been reported for multilayer graphene stacks on the carbon face of the substrate.^{19,20} The need for quality control of SiC/G derives from the modification of the SiC surface during high-temperature annealing. The surface of silicon carbide reconstructs during high-temperature annealing, leading to the appearance of stepped terraces and nucleation of multilayer graphene domains. These topographic features introduce electron scattering and lead to uneven doping profiles, which limit the performance of SiC/G electronic devices and prevent their large-scale integration.²¹ Scanning probe microscopy techniques (SPM) and Raman spectroscopy are often used for characterization of graphene layers, but they are time-consuming.^{22–25} Alternative characterization methods, such as those that irradiate the delicate graphene monolayer with electrons, are often invasive, introducing uncontrolled dopants and scatterers in the graphene layer.²⁶ Furthermore, invasive characterization methods prevent the study of correlations between the as-grown SiC/G morphology and its electronic

Received: May 24, 2013

Revised: July 29, 2013

Published: August 13, 2013

properties. Establishing SiC/G as a wafer-scale technology would require a demonstration of structural and electronic homogeneity of the produced graphene monolayer on the same scale, preferably immediately after graphene growth. Alternatively, such strict growth requirements might be relaxed by the development of noninvasive quality control methods that allow placement of devices in optimal wafer positions to avoid defects.

Here we show that, contrary to widespread belief, the observation of nanoscopic features in SiC/G is possible in a simple setup consisting of an optical microscope equipped with just a standard halogen lamp and a computer interface. Light-transmission mode enables the identification of single- and multilayer graphene domains, as well as vicinal substrate steps. Reflection mode, on the other hand, provides higher contrast imaging of the steps by utilizing interference effects. Although possible through the eyepiece, the identification of multilayer domains on SiC/G is sped up by real-time contrast enhancement to increase the dynamic range of the image on a computer display. The small optical contrast from a single layer of graphene may be enhanced up to an order of magnitude in this way, enabling the possibility of wafer scale characterization. Steps on SiC become observable in transmission mode when the focal plane is set a few micrometers above or below the surface. We have also employed differential interference contrast microscopy (DIC) in reflection mode to improve the contrast and observe subnanometer features on the surface.^{27,28} In this study of correlation between the morphology of epitaxial graphene morphology and its electronic transport properties we describe four large-area SiC/G samples ($7 \times 7 \text{ mm}^2$). We focus on graphene grown at high temperature ($T = 2000 \text{ }^\circ\text{C}$) and 1 atm argon on the Si-terminated face (0001) of semi-insulating SiC (Cree, miscut angle <0.05), which is the technology of choice for most high-performance epitaxial graphene electronic devices.^{10–16} For electrical characterization we patterned Hall bar devices of different sizes ($180 \mu\text{m} \times 50$ to $8 \mu\text{m} \times 2 \mu\text{m}$) using standard electron beam lithography and oxygen plasma etching as described elsewhere.^{15,29} In addition to these four samples, we have characterized different types of SiC/G samples (see Supporting Information) including monolayer on the Si-face, multilayer on the C-face, quasi-free-standing (hydrogen intercalated) monolayer on the Si-face, and also graphene grown on conductive (n+) SiC. The samples have been imaged prior to, during, and after microfabrication without loss of contrast in the presence of thick polymer resists ($\sim 0.6 \mu\text{m}$) or contamination from polymer residues.

Optical imaging has allowed us to study the correlation between the electronic properties of SiC/G with features produced on the substrate during growth. With this method we are able to inspect as-grown SiC/G samples and find suitable wafer positions where devices can be patterned. The position and orientation of devices on SiC/G wafer can have, under certain circumstances, profound implications on their performance. For example, Figure 1a shows a Hall bar that has been deliberately patterned in a region of the wafer which is free from multilayer domains; Figure 1b, on the other hand, shows a Hall bar that contains a bilayer graphene patch crossing the bar channel. Both Hall bars were fabricated on the same chip (sample SiC/G #1), and therefore the graphene layer has been grown under identical conditions. To compare both devices in terms of electronic properties we encapsulated the devices with photosensitive polymers, tuned their carrier concentration by

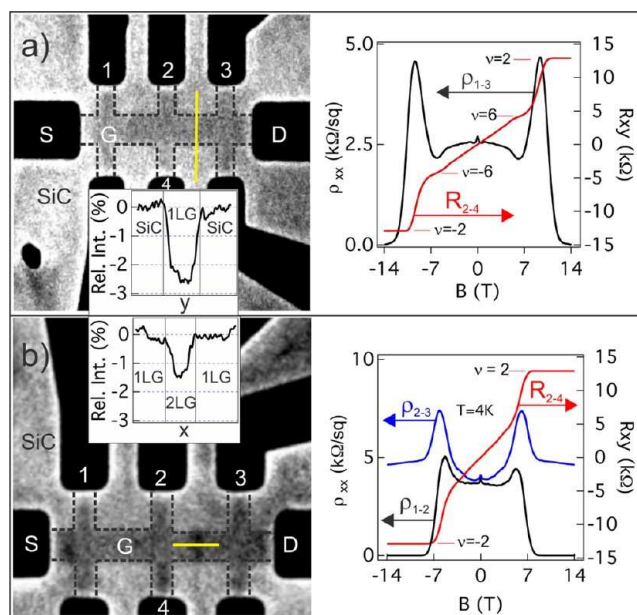


Figure 1. Use of optical microscopy to identify individual graphene layers on the surface of sample SiC/G #1. (a) Hall bar ($2 \times 8 \mu\text{m}^2$) consisting entirely of monolayer graphene, as revealed by the observation of fully developed half-integer quantum Hall effect. The inset is the measured relative intensity of light transmitted through SiC and graphene in the area shown by the yellow vertical line. (b) Hall bar containing mono- and bilayer graphene domains; while the longitudinal resistance in quantizing conditions is $\rho_{1-2} \sim 0$ for the purely monolayer region, the minimum resistance across the bilayer graphene domains is $\rho_{2-3} \sim 4.5 \text{ k}\Omega$. Inset: relative light intensity transmitted through a single layer compared to bilayer graphene on SiC. The images of the Hall bars obtained by optical microscopy have been separately contrast-enhanced for presentation purposes in order to compensate for illumination artifacts introduced by the neighboring metallic contacts (e.g. see the bright perimeter of the contacts).

irradiating them with ultraviolet light,²⁹ and performed magneto-transport measurements. At low temperatures, the monolayer nature of the patch-free structure was revealed by the observation of half-integer quantum Hall effect (QHE) (Figure 1a), which is the fingerprint of monolayer graphene in magneto transport.^{2,3} Under quantizing conditions, the quasi-relativistic nature of carriers in graphene is manifested in an anomalous set of Hall plateaux, $R_H = (h/4e^2)(n + 1/2)^{-1}$, with h the Planck constant, e the elementary charge, and n integer, zero included. Resistance plateaux at the filling factor $\nu = 4(n + 1/2) = 2, 6$ (corresponding to $n = 0, 1$) are visible, and the sample enters the nondissipative quantum Hall state, once the longitudinal resistivity along the entire channel is $\rho_{13} = 0$, at magnetic fields $B \sim 14 \text{ T}$. Significantly, a vanishing resistance is also measured in the Hall bar containing a patch as long as the longitudinal voltage is measured in the purely monolayer region (Figure 1b, terminals 1–2). However, when the longitudinal voltage is measured across the bilayer patch, we observed a large longitudinal resistivity $\rho_{23} \approx 4.5 \text{ k}\Omega$ at the maximum field in our setup ($B = 14 \text{ T}$). Previous reports of quantum transport in SiC/G attributed similar behavior to the presence of terraces perpendicular to the Hall bar channel.³⁰ However, in our measurements the bilayer-free Hall bar is also oriented perpendicular to terraces on SiC ($\sim 1 \text{ nm}$ high), and we have observed a fully developed half-integer QHE. The nonvanishing longitudinal resistance is thus attributed to the bilayer domain

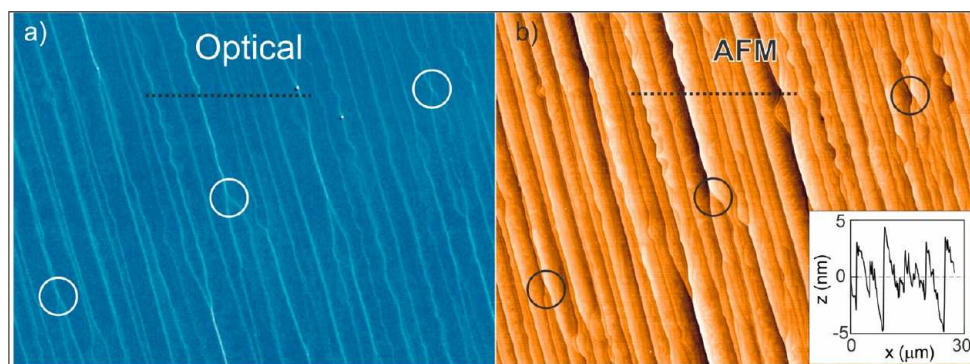


Figure 2. Observation of stepped terraces on the surface of sample SiC/G #2 by differential interference contrast microscopy (DIC) (a) and atomic force microscopy (AFM) in tapping mode. (b) Three distinctive topographical features are encircled for comparison. The inset shows the surface height along the dashed line ($30 \mu\text{m}$). While 5 nm high steps are easily identified, the minimum observable height feature using an optical microscope is below 1 nm .

crossing the Hall bar channel, which behaves as a metallic short that couples opposite edge states via transverse transport channels.³¹ This remarkable difference in performance for the two Hall bars stresses the importance of patterning graphene devices in suitable areas of SiC/G, especially when their dimensions are comparable to the typical size of multilayer domains on the chip.

We quantified the intensity of light transmitted through a single layer compared to that in silicon carbide as $\Delta I_{\text{ILG-SiC}} = (I_{\text{ILG}} - I_{\text{SiC}})/I_{\text{SiC}} = -(2.4 \pm 0.1)\%$ (inset in Figure 1a). The corresponding value between monolayer and a bilayer stripe is $\Delta I_{\text{2LG-1LG}} = -(1.3 \pm 0.2)\%$. Outside the uncertainty of our measurements we have not found any spread in the relative contrast measured in either reflection or transmission mode or by analyzing samples before or after patterning. The rapid identification of multilayer domains on SiC/G is facilitated by contrast enhancement. We employ a real-time gamma correction in software, such that the pixel intensity of the image displayed in the computer screen (I_{out}) is related to the sensor intensity (I_{in}) as $I_{\text{out}} \propto I_{\text{in}}^\gamma$, with $\gamma < 1$ (typically ~ 0.2 – 0.4). We emphasize that the measurements of relative intensity $\Delta I_{\text{ILG-SiC}}$ and $\Delta I_{\text{2LG-1LG}}$ do not include any contrast enhancement (gamma correction), which is only used to quickly identify multilayer domains on the SiC/G surface.

In general, the observation of atomically thin layers with an optical microscope can be explained by considering the strong light-graphene interaction: a freestanding monolayer blocks about 2.3% of incident light.³² In the case of SiC/G, the observation of monolayer is more challenging because the SiC substrate degrades the contrast roughly by a factor of 2 compared to graphene/vacuum interface. Employing a simple Fresnel model,³³ we estimated the optical contrast per graphene layer in reflection to be $(R - R_0)/R_0 \approx 1.5\%$ and $(T - T_0)/T_0 \approx 1.3\%$ for transmission mode (see Supporting Information). This value is in good agreement with the measured contrast between monolayer and bilayer (inset of Figure 1b). However, for the case of optical contrast between the SiC substrate and monolayer graphene grown on the Si face, the higher contrast can be explained by considering the presence of the buffer layer. Also referred to in literature as the zero-layer, this is a graphene-like layer covalently bonded to SiC that is a byproduct of graphene growth. The buffer is electrically insulating at low frequencies and therefore does not contribute to electron transport in DC measurements. However, since the buffer layer has a graphene-like structure

and the high-frequency (optical) conductance of a graphene stack consisting of N number of layers is very close to NG_0 ,^{32,33} we speculate that the observed higher optical contrast is due to the higher optical conductivity of the system composed of a buffer and a graphene monolayer ($N \sim 2$).

The optical characterization of SiC/G is complemented with the observation of stepped terraces on SiC and their impact on the electronic transport properties of graphene. We found that these topographic features are easily phase-imaged by DIC in reflection mode, and depending on their height and relative orientation they can affect the performance of the device to a different extent. Figure 2a,b shows the same area on a second sample (SiC/G #2) as imaged by DIC and atomic force microscopy (AFM); qualitatively, DIC images are remarkably similar to those obtained by AFM scans, and by direct comparison it is shown that, while heights $\geq 1 \text{ nm}$ are routinely observed, even subnanometer-range features on SiC can in principle be observed with this optical technique. In electron transport, we found that shallow steps (height $\sim 1 \text{ nm}$) have little impact on device performance. For instance, the device presented in Figure 1a was patterned oriented perpendicular to shallow stepped terraces, and half-integer QHE displayed by the device supports the idea of graphene following the substrate as a “smooth carpet over steps”. Nonetheless, we investigated further the effect of higher steps by using DIC imaging to identify terraces on the SiC/G #2 substrate prior to patterning. On this particular chip, chosen because it contained regions with shallow ($\sim 1 \text{ nm}$) and high ($\sim 20 \text{ nm}$) steps, Hall bars were patterned perpendicular or parallel to the stepped terraces. Again, in devices placed on shallow steps, we observed no difference in the transport properties, and the high-quality monolayer was confirmed by fully developed half-integer QHE; typical mobilities were of the order of ~ 2000 and as high as $6700 \text{ cm}^2 \text{ V}^{-1} \text{ s}^{-1}$ at liquid helium temperature (see the Supporting Information). The situation was substantially different when devices are patterned on high terraces (Figure 3a); in this case the observed average carrier concentrations were systemically higher ($n \approx 4 \times 10^{12} \text{ cm}^{-2}$), and the corresponding mobility was lower ($\mu \approx 600 \text{ cm}^2 \text{ V}^{-1} \text{ s}^{-1}$) irrespective of device orientation. We confirmed the effect of high terraces on a device fabricated right at the onset of high steps (Figure 3b). This device allowed the effect of step height to be compared on the same device. Step heights measured by AFM at the three crosses of the Hall bar were about 1 nm , 5 nm , and 20 nm , respectively. The as-fabricated carrier

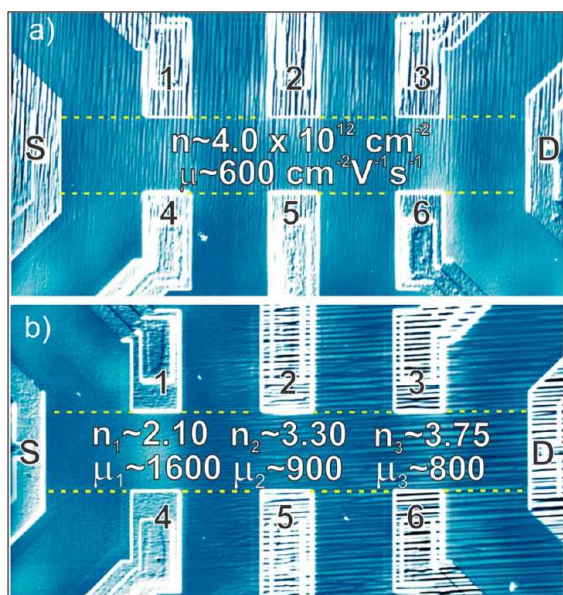


Figure 3. Studies of correlation between stepped terraces on sample SiC/G #2 and electronic properties enabled by optical microscopy and Hall effect measurements. (a) For Hall bars ($50 \times 180 \mu\text{m}^2$, indicated by dashed yellow line) patterned perpendicular to high terraces (height $\sim 20 \text{ nm}$), the average carrier concentrations and mobilities were found to be higher compared to devices patterned on shallow terraces (height $\sim 1 \text{ nm}$) on the same chip ($n \sim 4 \times 10^{12} \text{ cm}^{-2}$ and $\mu = 600 \text{ cm}^2 \text{ V}^{-1} \text{ s}^{-1}$). In measurements, current flows from source (S) to drain (D) and the Hall voltage is measured in terminals $V_{H1} = V_1 - V_4$, $V_{H2} = V_2 - V_5$, and $V_{H3} = V_3 - V_6$ in magnetic fields up to $B = 1 \text{ T}$. Carrier concentrations are calculated as $n = 1/eR_H$. (b) Large-area Hall bar ($50 \times 180 \mu\text{m}^2$) patterned parallel to terraces on SiC, at the onset of high steps. The carrier concentrations, shown in units of $10^{12} \text{ electron}\cdot\text{cm}^{-2}$, were measured to be higher as the step height increased. The maximum mobility corresponds to the region with shallowest steps.

concentrations for these three regions was measured through low-field Hall as $n = 1/eR_H$ and found to increase from $n_1 \approx 2.1 \times 10^{12} \text{ cm}^{-2}$ to $n_3 \approx 3.75 \times 10^{12} \text{ cm}^{-2}$; the corresponding mobilities decreased from $\mu_1 \approx 1600 \text{ cm}^2 \text{ V}^{-1} \text{ s}^{-1}$, to $\mu_3 \approx 860$

$\text{cm}^2 \text{ V}^{-1} \text{ s}^{-1}$. We propose that the source of the increased electron doping at higher steps is the more dense surface coverage by bilayer graphene confirmed by OM (see the Supporting Information), since high steps on SiC serve as nucleating centers for the growth of multilayer domains. The high-quality graphene on our samples is achieved because the majority of the steps created on the 4H SiC polytype during growth at high temperature and Ar pressure are 0.5 nm ($\sim 35\%$) and 1 nm ($\sim 25\%$).³⁴

In addition to the identification of terraces by exploiting interference effects in DIC imaging, we show that it is possible to obtain quantitative data about unit cell-high steps on SiC. While DIC imaging provides high contrast of subnanometer features, it does not provide directly quantitative information since the contrast observed in the image is not linearly proportional to the phase information. To obtain quantitative information we employed transport of intensity (TI) analysis in transmission mode,³⁵ which permits the retrieval of phase information from the difference between an in-focus image and a slightly defocused image (see the Supporting Information). For SiC/G we found that the optical contrast of nanometer-high steps is indeed enhanced by setting the focal plane about a micrometer above or below the surface. When the focus is above the surface (front focus), a bright-dark doublet is observed at the step edges, but the situation is reversed (bright and dark switch positions) when the focus is set below the surface (back focus). A TI analysis performed by taking just two intensity images at different z -planes ($\Delta z = 1.5 \mu\text{m}$) revealed that the minimum step height that we can reliably resolve is $\sim 1\text{--}3 \text{ nm}$, as confirmed by AFM scans on the same position of the sample (Figure 4a,b). Compared to AFM, the advantage of TI stems from its simplicity and speed, since it only requires the subtraction of two images obtained by setting the focus a known distance above and below the SiC/G surface. No further rescaling or calibration is required as we confirmed by direct comparison of AFM and TI in Figure 4a,b (see script for analysis in the Supporting Information).

Overall, optical imaging could be used to complement or even replace established characterization methods such as low energy electron microscopy (LEEM) or scanning probe

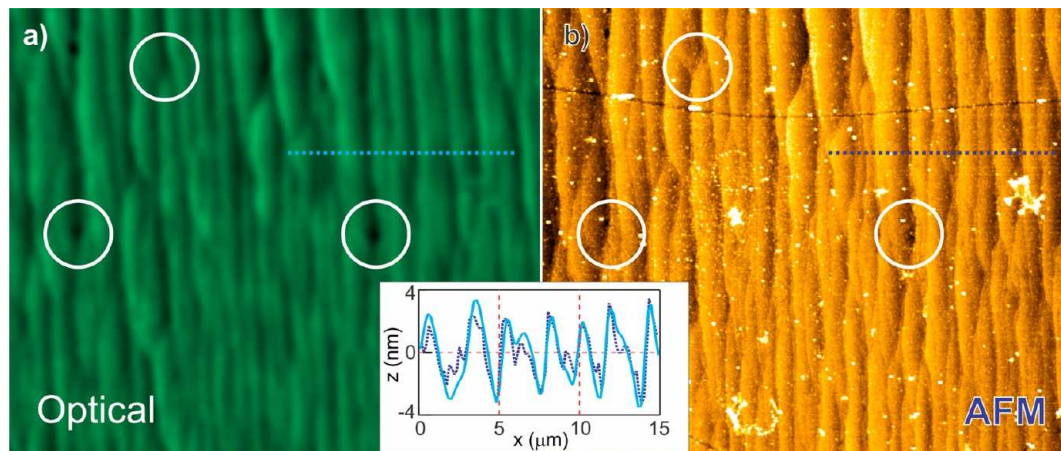


Figure 4. Imaging of nanometer high terraces on the surface of sample SiC/G #2. (a) The transport of intensity analysis allows one to obtain quantitative information about SiC topography down to $\sim 2 \text{ nm}$, as confirmed by atomic force microscopy (AFM) in tapping mode. (b) Three distinctive features in topography are encircled for comparison. The inset shows the surface height along the dashed line ($15 \mu\text{m}$) obtained by AFM (dark-blue dashed line) and transport of intensity analysis (light-blue line). The line profile corresponding to TI shows that the lateral resolution is about $1 \mu\text{m}$ (diffraction limited).

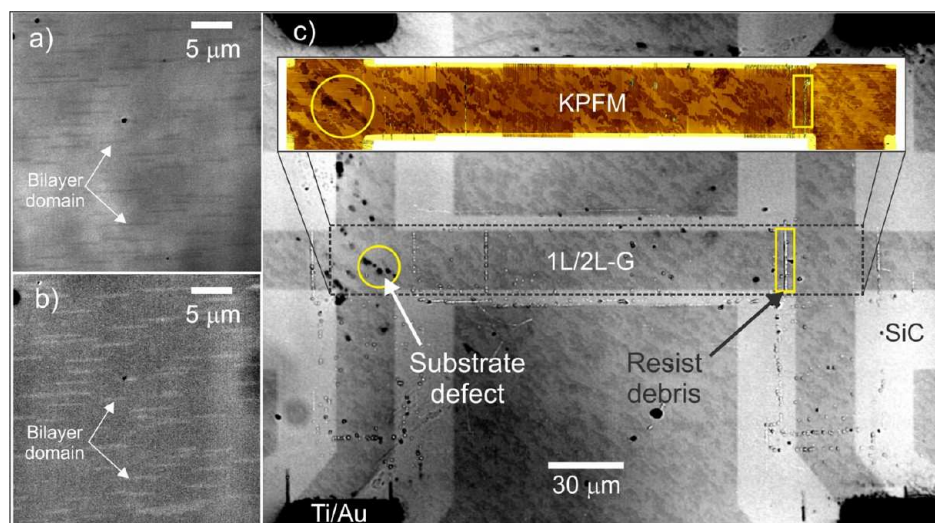


Figure 5. Observation of single and bilayer graphene domains on SiC/G. (a) Image taken in an optical microscope in transmission mode, arrows point at two bilayer patches appearing as dark stripes due to stronger light absorption. (b) In reflection mode, the contrast is inverted: bilayer graphene domains appear brighter. Both images obtained by optical microscopy have been contrast-enhanced for presentation purposes. (c) An optical microscopy (OM) image (transmission) of an electron-beam fabricated Hall bar ($24 \times 120 \mu\text{m}^2$) on SiC/G #4. The brightest regions in the optical image correspond to bare SiC accessible after etching of graphene during the last micro fabrication step. Dark areas in the corners of the image correspond to metallic contacts. The inset shows a Kelvin probe force microscopy (KPFM) image of the same device obtained prior to optical imaging. Resist debris resulting from AFM cleaning are observable in the OM image (e.g., yellow rectangle). On both OM and KPFM images, the bright contrast corresponds to a single layer and dark to a bilayer graphene.

microscopy (SPM). OM of multilayer graphene domains on SiC/G results in images that qualitatively resemble those obtained by LEEM,^{18,36,37} showing that similar information can be obtained in a much simpler way. Figure 5a shows an image of a nominally monolayer graphene for sample SiC/G #3 obtained in the light transmission mode. In this image the brighter area is monolayer graphene, and the dark stripes, where light is more strongly attenuated, correspond to bilayer graphene domains oriented along the terraces on SiC. In the case of imaging in reflection mode, the tone is inverted as shown in Figure 5b: bilayer graphene stripes appear brighter, and monolayer graphene appears darker. SPM techniques can provide quantitative information about the SiC surface or even about the number of graphene layers as in the case of Kelvin probe force microscopy (KPFM).^{38,39} Figure 5c shows a direct comparison of an epitaxial graphene structure patterned by electron beam lithography on SiC/G #4 as imaged by both KPFM (inset) and OM. Since KPFM maps the surface potential it has better performance when samples are free of any contamination. To obtain the surface potential map of Figure 5c, the graphene surface was cleaned of organic resist residuals using relatively slow contact mode AFM cleaning (i.e., ~ 1000 s per $100 \mu\text{m}^2$ scan).⁴⁰ In comparison, OM requires no special preprocessing as demonstrated on both the channel area, which is free of resist, and to the rest of the sample, which is contaminated with resist residues. OM can be regarded as an instantaneous way of obtaining qualitatively similar information as KPFM and LEEM, especially if the minimum feature size is above the diffraction limit; in this regard, the minimum bilayer domain that we have reliably imaged is about $1 \mu\text{m}$ (see Supporting Information).

In summary we demonstrate a simple technique for rapid characterization of graphene grown on silicon carbide. This method gives qualitatively similar information about the topography and layer coverage to that obtained by LEEM, AFM, and KPFM but in a much faster and noninvasive way.

This is crucial for the design of epitaxial graphene devices with optimal performance. The use of optical microscopy has helped us understand the correlation between morphology of SiC/G and its electronic properties. We have shown that a single layer of graphene on SiC can be identified using optical microscopy and proved its monolayer nature by the observation of half-integer quantum Hall effect. We also demonstrated that unit-cell high terraces in our samples are not detrimental for electronic properties of epitaxial graphene on SiC, but bilayer domains are. The presence of bilayer domains on our samples is minimized because the majority of the steps created on the 4H SiC polytype during growth at high temperature/pressure are maximum one unit cell. Optical microscopy can serve as an enabling technology for material scientists to study the formation of defects on SiC/G during growth (stepped terraces and multilayer domains) on the way toward a wafer scale production of epitaxial graphene.

■ ASSOCIATED CONTENT

📄 Supporting Information

Details of sample patterning, analysis of lateral resolution of optical microscopy, theoretical values of absorption and transmission coefficients of monolayer graphene on SiC, details of the transport of analysis (TI) including script, half-integer quantum Hall effect in a stepped substrate, and examples of optical images for different SiC/G substrates. This material is available free of charge via the Internet at <http://pubs.acs.org>.

■ AUTHOR INFORMATION

Corresponding Author

*Tel.: +46 31 772 3031. Fax: +46 31 772 3471. E-mail: samuel.lara@chalmers.se.

Author Contributions

T.Y. and A.L. contributed equally.

Notes

The authors declare no competing financial interest.

ACKNOWLEDGMENTS

This work was supported by EU FP7 project ConceptGraphene, Swedish Research Council and Foundation for Strategic Research, The Knut and Alice Wallenberg Foundation (KAW), IRD graphene project of the UK National measurement office. The authors are grateful to Tord Claeson, Mikael Käll, and John Gallop for illuminating discussions and careful reading of the manuscript.

REFERENCES

- (1) Novoselov, K. S.; Geim, A. K.; Morozov, S. V.; Jiang, D.; Zhang, Y.; Dubonos, S. V.; Grigorieva, I. V.; Firsov, A. A. Electric Field Effect in Atomically Thin Carbon Films. *Science* **2004**, *306*, 666–9.
- (2) Zhang, Y.; Tan, Y.-W.; Stormer, H. L.; Kim, P. Experimental Observation of the Quantum Hall Effect and Berry's Phase in Graphene. *Nature* **2005**, *438*, 201–4.
- (3) Novoselov, K. S.; Geim, A. K.; Morozov, S. V.; Jiang, D.; Katsnelson, M. I.; Grigorieva, I. V.; Dubonos, S. V.; Firsov, A. A. Two-dimensional Gas of Massless Dirac Fermions in Graphene. *Nature* **2005**, *438*, 197–200.
- (4) Roddaro, S.; Pingue, P.; Piazza, V.; Pellegrin, V.; Beltram, F. The Optical Visibility of Graphene: Interference Colors of Ultrathin Graphite on SiO₂. *Nano Lett.* **2007**, *7*, 2707–2710.
- (5) Blake, P.; Hill, E. W.; Neto, A. H.; Novoselov, K. S.; Jiang, D.; Yang, R.; Booth, T. J.; Geim, A. K. Making Graphene Visible. *Appl. Phys. Lett.* **2007**, *91*, 63124.
- (6) Nolen, C. M.; Denina, G.; Teweldebrhan, D.; Bhanu, B.; Balandin, A. A. High-throughput Large-area Automated Identification and Quality Control of Graphene and Few-layer Graphene Films. *ACS Nano* **2011**, *5*, 914–22.
- (7) Yu, Q.; Jauregui, L. A.; Wu, W.; Colby, R.; Tian, J.; Su, Z.; Cao, H.; Liu, Z.; Pandey, D.; Wei, D.; et al. Control and Characterization of Individual Grains and Grain Boundaries in Graphene Grown by Chemical Vapour Deposition. *Nat. Mater.* **2011**, *10*, 443–9.
- (8) Wu, Y. Q.; Ye, P. D.; Capano, M. A.; Xuan, Y.; Sui, Y.; Qi, M.; Cooper, J. A.; Shen, T.; Pandey, D.; Prakash, G.; et al. Top-gated Graphene Field-effect-transistors Formed by Decomposition of SiC. *Appl. Phys. Lett.* **2008**, *92*, 092102.
- (9) Kedzierski, J.; Hsu, P. L.; Healey, P.; Wyatt, P. W.; Keast, C. L.; Sprinkle, M.; Berger, C.; de Heer, W. A. Epitaxial Graphene Transistors on SiC Substrates. *IEEE Trans. Electron Devices* **2008**, *55*, 2078–2085.
- (10) Lin, Y. M.; Dimitrakopoulos, C.; Jenkins, K. A.; Farmer, D. B.; Chiu, H. Y.; Grill, A.; Avouris, P. 100-GHz Transistors from Wafer-scale Epitaxial Graphene. *Science* **2010**, *327*, 662.
- (11) Panchal, V.; Cox, D.; Yakimova, R.; Kazakova, O. Epitaxial Graphene Sensors for Detection of Small Magnetic Moments. *IEEE Trans. Magn.* **2013**, *49*, 97–100.
- (12) Kazakova, O.; Panchal, V.; Burnett, T. Epitaxial Graphene and Graphene-Based Devices Studied by Electrical Scanning Probe Microscopy. *Crystals* **2013**, *3*, 191–233.
- (13) Nomani, M. W. K.; Shishir, R.; Qazi, M.; Diwan, D.; Shields, V. B.; Spencer, M. G.; Tompa, G. S.; Sbrockey, N. M.; Koley, G. Highly Sensitive and Selective Detection of NO₂ Using Epitaxial Graphene on 6H-SiC. *Sens. Actuators, B* **2010**, *150*, 301–307.
- (14) Pearce, R.; Iakimov, T.; Andersson, M.; Hultman, L.; Spetz, A. L.; Yakimova, R. Epitaxially Grown Graphene Based Gas Sensors for Ultra Sensitive NO₂ Detection. *Sens. Actuators, B* **2011**, *155*, 451–455.
- (15) Tzalenchuk, A.; Lara-Avila, S.; Kalaboukhov, A.; Paolillo, S.; Syväjärvi, M.; Yakimova, R.; Kazakova, O.; Janssen, T. J. B. M.; Fal'ko, V.; Kubatkin, S. Towards a Quantum Resistance Standard Based on Epitaxial Graphene. *Nat. Nanotechnol.* **2010**, *5*, 186–9.
- (16) Janssen, T. J. B. M.; Williams, J. M.; Fletcher, N. E.; Goebel, R.; Tzalenchuk, A.; Yakimova, R.; Lara-Avila, S.; Kubatkin, S.; Fal'ko, V. I. Precision Comparison of the Quantum Hall Effect in Graphene and Gallium Arsenide. *Metrologia* **2012**, *49*, 294–306.
- (17) Abergel, D.; Russell, A.; Falko, V. Visibility of Graphene Flakes on a Dielectric Substrate. *Appl. Phys. Lett.* **2007**, *91*, 063125.
- (18) Gaskell, P. E.; Skulason, H. S.; Rodenchuk, C.; Szkopek, T. Counting Graphene Layers on Glass via Optical Reflection Microscopy. *Appl. Phys. Lett.* **2009**, *94*, 143101.
- (19) Camara, N.; Huntzinger, J. R.; Rius, G.; Tiberj, A.; Mestres, N.; Pérez-Murano, F.; Godignon, P.; Camassel, J. Anisotropic Growth of Long Isolated Graphene Ribbons on the C Face of Graphite-capped 6H-SiC. *Phys. Rev. B* **2009**, *80*, 125410.
- (20) Camara, N.; Tiberj, A.; Jouault, B.; Caboni, A.; Jabkhanji, B.; Mestres, N.; Godignon, P.; Camassel, J. Current Status of Self-organized Epitaxial Graphene Ribbons on the C Face of 6H-SiC Substrates. *J. Phys. D: Appl. Phys.* **2010**, *43*, 374011.
- (21) Ji, S. H.; Hannon, J. B.; Tromp, R. M.; Perebeinos, V.; Tersoff, J.; Ross, F. M. Atomic-scale Transport in Epitaxial Graphene. *Nat. Mater.* **2011**, *11*, 114.
- (22) Fromm, F.; Oliveira, M. H.; Molina-Sánchez, A.; Hundhausen, M.; Lopes, J. M. J.; Riechert, H.; Wirtz, L.; Seyller, T. Contribution of the Buffer Layer to the Raman Spectrum of Epitaxial Graphene on SiC(0001). *New J. Phys.* **2013**, *15*, 043031.
- (23) Graf, D.; Molitor, F.; Ensslin, K.; Stampfer, C.; Jungen, A.; Hierold, C.; Wirtz, L. Spatially Resolved Raman Spectroscopy of Single- and Few-layer Graphene. *Nano Lett.* **2007**, *7*, 238–42.
- (24) Lee, D. S.; Riedl, C.; Krauss, B.; von Klitzing, K.; Starke, U.; Smet, J. H. Raman Spectra of Epitaxial Graphene on SiC and of Epitaxial Graphene Transferred to SiO₂. *Nano Lett.* **2008**, *8*, 4320–5.
- (25) Ni, Z.; Chen, W.; Fan, X.; Kuo, J.; Yu, T.; Wee, A.; Shen, Z. Raman Spectroscopy of Epitaxial Graphene on a SiC Substrate. *Phys. Rev. B* **2008**, *77*, 115416.
- (26) Tao, L.; Qiu, C.; Yu, F.; Yang, H. Modification on Single-Layer Graphene Induced by Low-Energy Electron-Beam Irradiation. *J. Phys. Chem. C* **2013**, *117*, 10079–85.
- (27) Nomarski, G. Differential Microinterferometer with Polarized Waves. *J. Phys. Radium* **1955**, *16*, 9S–11S.
- (28) Allen, R. D.; David, G. B.; Nomarski, G. The Zeiss-Nomarski Differential Interference Equipment for Transmitted-light Microscopy. *Z. Wiss. Mikroskop.* **1969**, *69*, 193.
- (29) Lara-Avila, S.; Moth-Poulsen, K.; Yakimova, R.; Bjørnholm, T.; Fal'ko, V.; Tzalenchuk, A.; Kubatkin, S. Non-Volatile Photochemical Gating of an Epitaxial Graphene/Polymer Heterostructure. *Adv. Mater.* **2011**, *23*, 878–882.
- (30) Schumann, T.; Friedland, K. J.; Oliveira, M. H.; Tahraoui, A.; Lopes, J. M. J.; Riechert, H. Anisotropic Quantum Hall Effect in Epitaxial Graphene on Stepped SiC Surfaces. *Phys. Rev. B* **2012**, *85*, 235402.
- (31) Tomas, L.; San-jose, P.; Prada, E. Quantum Hall Effect in Graphene with Twisted Bilayer Stripe Defects. *Phys. Rev. B* **2013**, *87*, 205429.
- (32) Nair, R.; Blake, P.; Grigorenko, A.; Novoselov, K. S.; Booth, T.; Stauber, T.; Pers, N.; Geim, A. K. Fine Structure Constant Defines Visual Transparency of Graphene. *Science* **2008**, *320*, 1308.
- (33) Stauber, T.; Peres, N. M. R.; Geim, A. K. Optical Conductivity of Graphene in the Visible Region of the Spectrum. *Phys. Rev. B* **2008**, *78*, 85432.
- (34) Yazdi, R.; Vasiliaskas, R.; Iakimov, T.; Zakharov, A.; Syväjärvi, M.; Yakimova, R. Growth of Large Area Monolayer Graphene on 3C-SiC and a Comparison with Other SiC Polytypes. *Carbon* **2013**, *57*, 477.
- (35) Streibl, N. Phase Imaging by the Transport Equation of Intensity. *Opt. Commun.* **1984**, *49*, 6–10.
- (36) Virojanadara, C.; Syväjärvi, M.; Yakimova, R.; Johansson, L.; Zakharov, A.; Balasubramanian, T. Homogeneous Large-area Graphene Layer Growth on 6H-SiC(0001). *Phys. Rev. B* **2008**, *78*, 1–6.
- (37) Ohta, T.; El Gabaly, F.; Bostwick, A.; McChesney, J. L.; Emtsev, K. V.; Schmid, A. K.; Seyller, T.; Horn, K.; Rotenberg, E. Morphology

of Graphene Thin Film Growth on SiC(0001). *New J. Phys.* **2008**, *10*, 023034.

(38) Burnett, T.; Yakimova, R.; Kazakova, O. Identification of Epitaxial Graphene Domains and Adsorbed Species in Ambient Conditions Using Quantified Topography Measurements. *J. Appl. Phys.* **2012**, *112*, 54307–8.

(39) Burnett, T.; Yakimova, R.; Kazakova, O. Mapping of Local Electrical Properties in Epitaxial Graphene Using Electrostatic Force Microscopy. *Nano Lett.* **2011**, *11*, 2324–8.

(40) Lindvall, N.; Kalabukhov, A.; Yurgens, A. Cleaning Graphene Using Atomic Force Microscope. *J. Appl. Phys.* **2012**, *111*, 064904.